

Tracking a complete voltage-sensor cycle with metal-ion bridges

Ulrike Henrion, Jakob Renhorn, Sara Börjesson, Erin M Nelson, Christine S Schwaiger, Par Bjelkmar, Björn Wallner, Erik Lindahl and Fredrik Elinder

Linköping University Post Print

N.B.: When citing this work, cite the original article.

Original Publication:

Ulrike Henrion, Jakob Renhorn, Sara Börjesson, Erin M Nelson, Christine S Schwaiger, Par Bjelkmar, Björn Wallner, Erik Lindahl and Fredrik Elinder, Tracking a complete voltage-sensor cycle with metal-ion bridges, 2012, Proceedings of the National Academy of Sciences of the United States of America, (109), 22, 8552-8557.

<http://dx.doi.org/10.1073/pnas.1116938109>

Copyright: National Academy of Sciences

<http://www.nas.edu/>

Postprint available at: Linköping University Electronic Press

<http://urn.kb.se/resolve?urn=urn:nbn:se:liu:diva-78812>

CLASSIFICATION: BIOLOGICAL SCIENCES – Biophysics and Computational Biology

Tracking a complete voltage-sensor cycle with metal-ion bridges

Ulrike Henrion^a, Jakob Renhorn^a, Sara I. Börjesson^a, Erin M. Nelson^a, Christine S. Schwaiger^b, Pär Bjelkmar^{b,c}, Björn Wallner^d, Erik Lindahl^{b,c,1}, and Fredrik Elinder^{a,1}

^aDivision of Cell Biology, Department of Clinical and Experimental Medicine, Linköping University, SE-581 85 Linköping, Sweden.

^bTheoretical & Computational Biophysics, Department of Theoretical Physics & Swedish e-Science Research Center, Royal Institute of Technology, SE-106 91 Stockholm, Sweden

^cCenter for Biomembrane Research, Department of Biochemistry & Biophysics, Stockholm University, SE-106 91 Stockholm, Sweden

^dDepartment of Physics, Chemistry and Biology & Swedish e-Science Research Center, Linköping University, SE-581 83 Linköping, Sweden

¹Address correspondence to:

Fredrik Elinder, Division of Cell Biology, Department of Clinical and Experimental Medicine, Linköping University, SE-581 85 Linköping, Sweden; Telephone: +46-101038945; FAX: +46-101033192; E-mail: fredrik.elinder@liu.se; Erik Lindahl, Theoretical & Computational Biophysics, Department of Theoretical Physics & Swedish e-Science Research Center, Royal Institute of Technology, 106 91 Stockholm, Sweden. E-mail: erik@kth.se

Key words: K channel, Molecular dynamics, Rosetta, Voltage clamp, voltage gating, 3₁₀-helix, conformational transition, gating model

Voltage-gated ion channels open and close in response to changes in membrane potential, thereby enabling electrical signaling in excitable cells. The voltage sensitivity is conferred through four voltage-sensor domains (VSDs), where positively charged residues in the fourth transmembrane segment (S4) sense the potential. While an open state is known from the Kv1.2/2.1 X-ray structure, the conformational changes underlying voltage sensing have not been resolved. Here, we present 20 new interactions in one open and four different closed conformations based on metal-ion bridges between all four segments of the VSD in the voltage-gated Shaker K channel. A subset of the experimental constraints was used to generate Rosetta models of the conformations, which were subject to molecular simulation and tested against the remaining constraints. This achieves a detailed model of intermediate conformations during VSD gating. The results provide molecular insight into the transition, suggesting that S4 slides at least 12 Å along its axis to open the channel with a 3₁₀-helix region present that moves in sequence in S4 in order to occupy the same position in space opposite F290 from the open through the three first closed states.

\body

Voltage-gated ion channels are critical for biological signaling and are able to regulate ion flux on a millisecond time scale. To sense changes in membrane voltage, each ion channel is equipped with four voltage-sensor domains (VSDs) connected to a central ion-conducting pore domain. The fourth transmembrane segment (S4) of each VSD carries several positively charged amino-acid residues responsible for VSD gating [1]. At least three elementary charges per VSD must traverse outwards through the membrane electric field to open a channel, which corresponds to a considerable displacement of the S4 helix (Fig. 1A) [2-4]. The positive charges in S4 make salt bridges with negative countercharges on their move through the VSD [4-8]. It has even been proposed that the VSD undergoes a conformational alteration following the opening, when the channel relaxes to an inactivated, that is closed, state [9]. In addition to conferring voltage dependence to ion channels, VSDs also regulate enzymes [10], act as voltage-gated proton channels [11, 12], are susceptible to disease-causing mutations [13, 14], and serve as target for drugs and toxins [1, 15-18]. It is therefore of crucial interest to understand the details underlying voltage sensing by VSDs.

Few, if any, segments of membrane proteins have received more attention than the S4 helix of voltage sensors. This is not only because of their paramount biological importance, but because they can help us understand fundamental biophysical problems such as why some membrane protein segments can be hydrophilic [19], how charges effectively move through a membrane, or how a potential triggers structural changes on a microsecond time scale. These questions are inherently linked to transient conformations and contacts that can be difficult to capture in a single structure. However, while active/open-state conformations are known at atomic resolution for both K and Na channels [5, 20], the structure of the resting state has not yet been determined experimentally, and our knowledge about the VSD gating processes, including inactivation, is limited. There is strong experimental data suggesting each voltage sensor (in particular the S4 helix) must adopt at least one intermediate state between the conducting and the resting state [3, 4, 21], which makes the pathway particularly interesting.

Structural constraints in a working ion channel can be explored by introducing pairs of cysteines that, if close enough, can be linked by disulfide bonds (Fig. 1B upper) to alter the ion channel kinetics [7, 8, 22, 23]. However, disulfide bonds have the disadvantage that cysteines up to 15 Å apart can be caught in a bond [24] and due to their high strength they could capture the channel in a non-natural, or at least less common, conformation. Therefore, in this study, we have used weaker Cd²⁺ bridges that are more likely to catch the channel in native conformations [25-28] (sulfur distances <6.5 Å [29]; Fig. 1B middle). In particular, their lower strength means the interactions can break and reform, which makes it possible to maintain the channel in a working state. Cd²⁺ bridges are normally formed between cysteines and histidines, but can also be formed between negatively charged glutamates and aspartates [29]. Additionally, here we also explore Cd²⁺ bridges between one cysteine and multiple glutamates or aspartates (Fig. 1B lower).

To search for possible interaction we used the voltage-gated Shaker K channel expressed in oocytes from the frog *Xenopus laevis*. Residues 325 and 326 in S3 are close to the gating charges R1 (=R362), R2 (=R365), and R3 (=R368) in S4 in the open state [23]. Therefore, to probe for movements within the VSD we first explored interactions between 325 or 326, and a long stretch of residues in S4 (355-369; green segment in Fig. 1C) using Cd²⁺ bridges. An interaction in a

non-conducting (closed, but not necessarily resting) state is expected to shift the voltage dependence of channel opening in positive direction along the voltage axis and to slow down opening (although by itself it does not distinguish between different closed states). Similarly, an interaction in the open state is expected to shift the voltage dependence in negative direction and to slow down closing (Fig. 1D-E). Out of 49 mutations investigated, 20 interactions were found. This investigation follows three steps: (i) We start by identifying several strong Cys-Cd²⁺-Cys bridges. Then (ii) we use these interactions to build molecular models. Finally (iii) we use several weaker Cys-Cd²⁺-Glu/Asp interactions to assess predictions generated by the models. These constraints and derived models provide detailed information covering a complete cycle of conformations for a voltage-sensor.

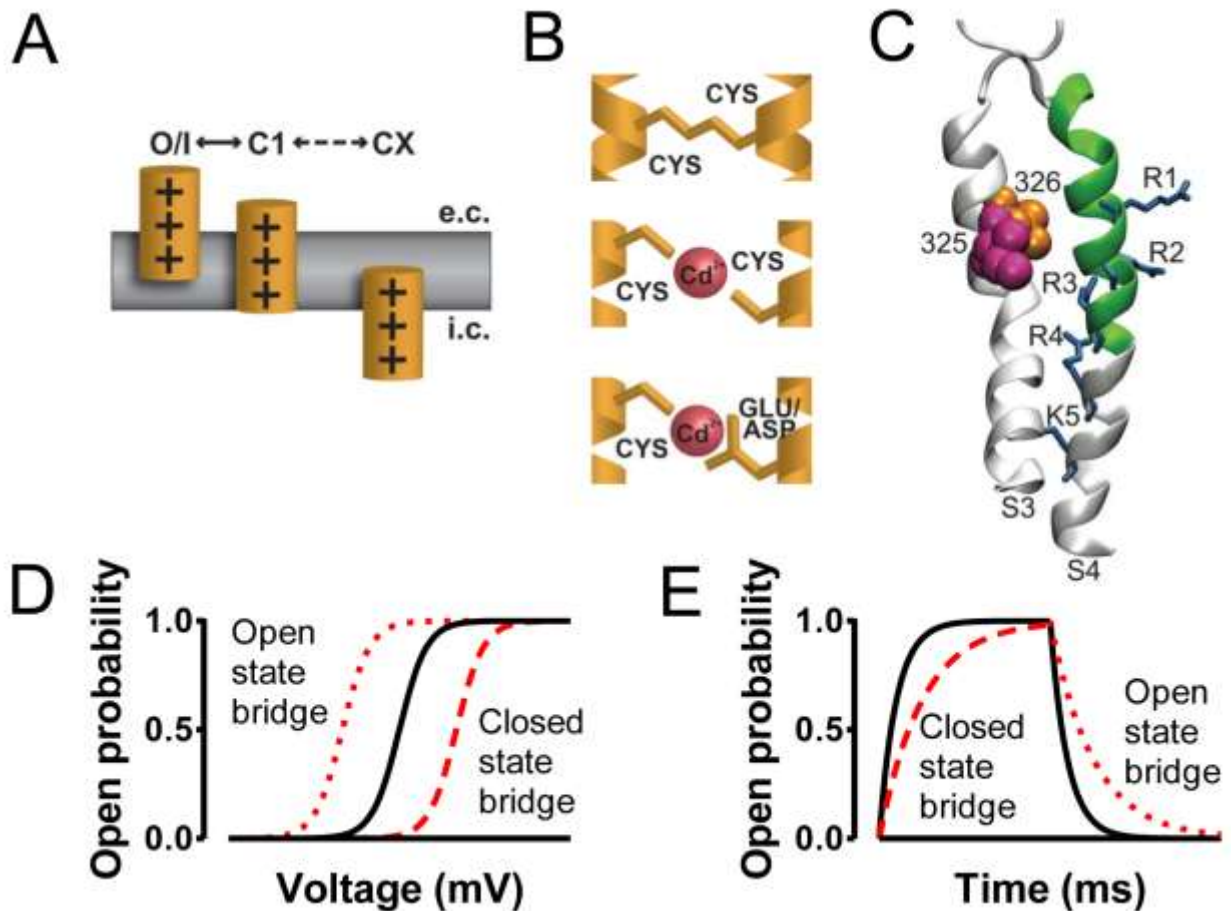


Fig. 1. Probing voltage sensor dynamics with Cd²⁺ bridges. (A) Multiple molecular states of the S4 voltage sensor. O, open; I, inactivated; C, closed states. (B) Three types of interactions. Covalent disulfide bonds (upper), Cd²⁺ bridges coordinating two cysteines (middle), and Cd²⁺ bridges coordinating one cysteine and two or several glutamates/aspartates (lower). (C) Residues 325 (magenta) and 326 (orange) are depicted as space-filling. Residues 355-369 (green) are investigated with respect to interactions with 325 and 326. Blue sticks represent the gating charges. (D-E), Possible effects of Cd²⁺ bridges (red) on voltage and time dependence of the open probability.

RESULTS

Residues 325C and 326C in S3 make close contact with a long stretch of residues in S4.

10 μM Cd^{2+} quickly (within 10-20 s) and almost completely reduced the current of 325C/358C at 100-ms long pulses to +20 mV (Fig. 2A-B, Fig. S1A for controls). Removal of Cd^{2+} did not restore the current within 10 min (Fig. 2B), but addition of the Cd^{2+} chelator EGTA reversed the effect (Fig. S1B). This suggests that at some point during channel gating, 325C and 358C are in close proximity, forming a metal-ion bridge between 325C and 358C with a low K_d value; 10 nM Cd^{2+} reduced the current by $36 \pm 12\%$ ($n = 4$). Seven other double mutants, but none of the single mutants, showed similar pronounced current reduction (Fig. 2C, Table S1). Longer and higher voltage pulses restored the current amplitudes and broke the bridges even in the presence of Cd^{2+} . Application of a 1-s long pulse to +50 mV in Cd^{2+} opened the channels, suggesting that these interactions occur in closed states of the channel. As expected for a closed-state interaction, the voltage dependence for opening was shifted by $+55 \pm 3$ mV ($n = 3$) (Fig. 3A), and the opening kinetics was slowed down by a factor of 490 ± 50 ($n = 3$) (Fig. 3B).

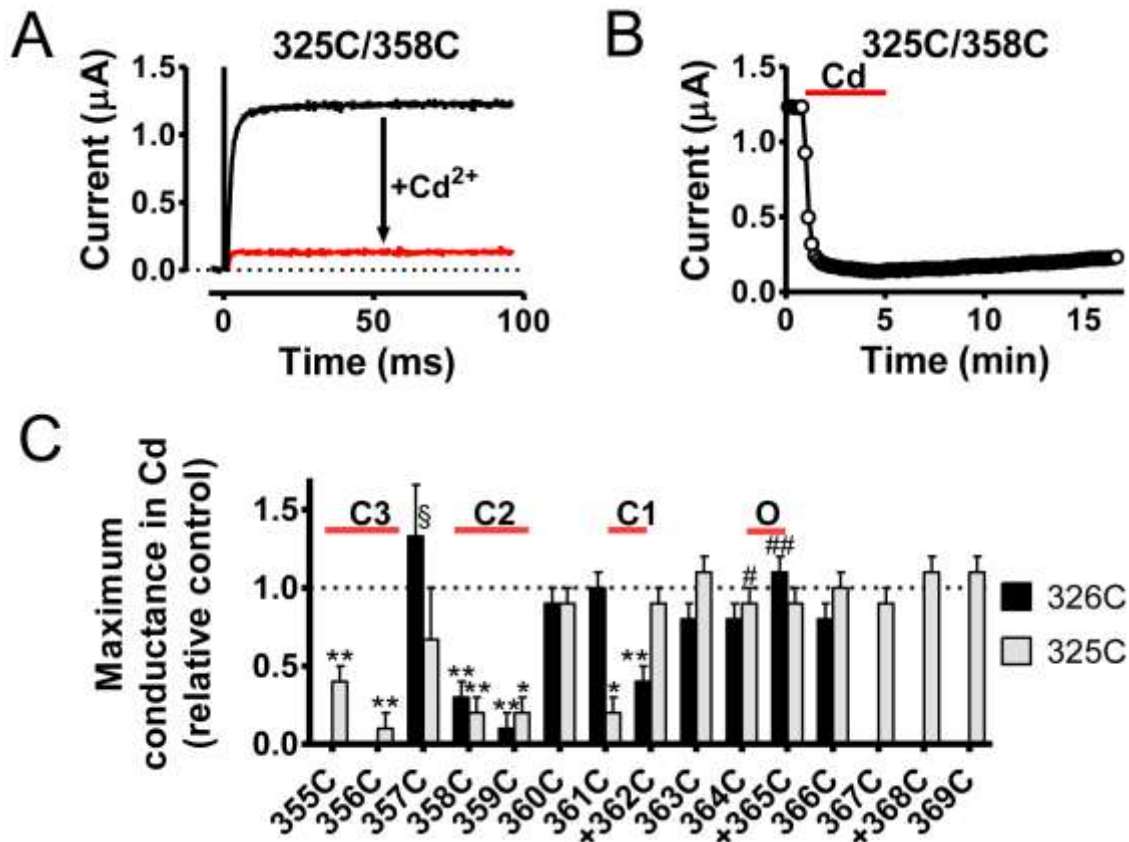


Fig. 2. Cd^{2+} bridges between 325C or 326C in S3 and residues in S4. (A) Cd^{2+} reduces the current amplitude of 325C/358C at +20 mV. Holding voltage -80 mV. (B) Bridge formation in 325C/358C occurs quickly after application of Cd^{2+} . Washout is very slow. (C) Cd^{2+} effects on maximum conductances (Table S1; $n = 2-12$). §: Data for 357 double mutants were divided by the effect on the single mutant 357C (Table S1). #, ##: open-state interactions 325C-364C and 326C-365C. C3, C2, C1 and O denote suggested states for the interactions. Data shown as mean \pm SEM. Amplitudes significantly different from 1.0 are denoted by * if $p < 0.05$ or ** if $p < 0.01$.

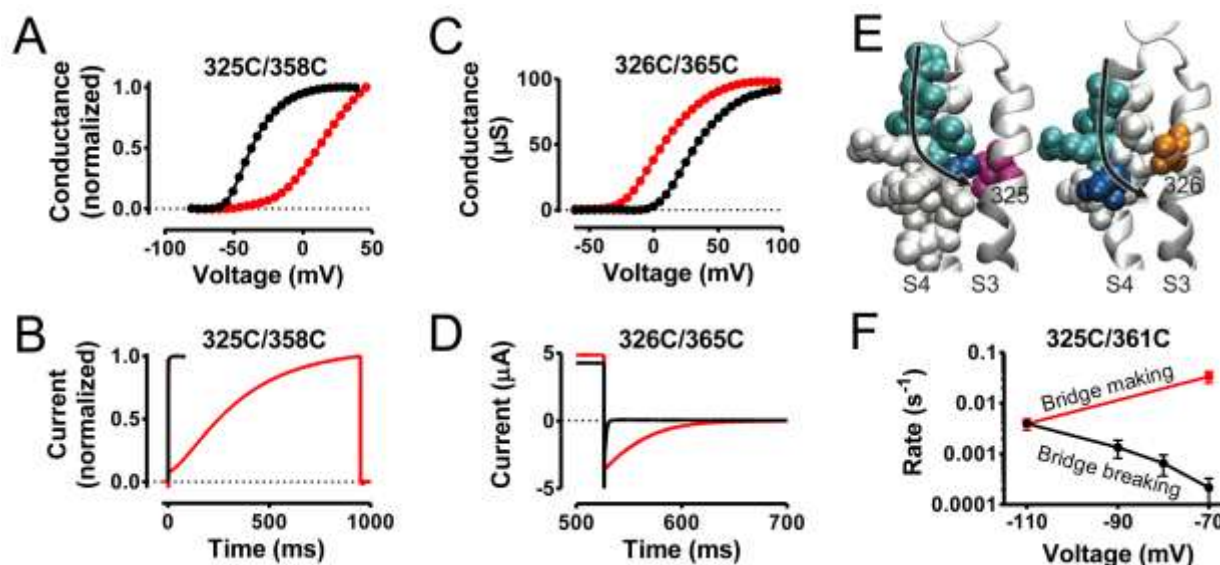


Fig. 3. State dependence of Cd^{2+} bridges. (A-B) Closed-state interaction in 325C/358C. Cd^{2+} shifts the $G(V)$ by +55 mV (A), and slows down channel opening at +50 mV by a factor of 490 (B). The maximum conductance was reduced by $54 \pm 7\%$ ($n = 3$). Cd^{2+} effects in red and control in black. (C-D) Open-state interaction in 326C/365C. Cd^{2+} shifts the $G(V)$ by -21 mV (C), and slows down channel closure by a factor of 31 in a high K^+ solution at -60 mV following a pulse to +60 mV (D). Cd^{2+} effects in red and control in black. (E) Summary of the interactions. Residues in S3 interacting with 325C (left) and 326C (right) respectively are shown in cyan (closed states) and blue (open state) in the Kv1.2/2.1 chimera structure (6). (F) Voltage-dependence of the kinetics of Cd^{2+} bridge making and breaking for 325C/361C. Data shown as mean \pm SEM ($n = 2-3$).

326C/365C and 325C/364C stabilize the open state. In addition to the clear current reductions shown in Fig. 2C, we found two double-cysteine mutations with Cd^{2+} bridges in the open state. Cd^{2+} opened 326C/365C by shifting the voltage dependence by -21 ± 1 mV ($n = 12$) (Fig. 3C), and slowed down the closing by a factor of 31 ± 6 ($n = 4$) (Fig. 3D). The interaction is fast (~200 ms) in the open state, suggesting that 326C and 365C are close to each other in the open-active state (Fig. S2). Most likely, the reason for the fast reaction is that Cd^{2+} is already in place, being attracted by neighboring glutamates in S1 (E247) and S2 (E283) and coordinated by 326C (Fig. S3). In the open-state crystal structure, 325 and 364 are very close to each other. However, the Cd^{2+} bridge formation was slower for 325C/364C than for 326C/365C, probably because of the lack of pre-bridge Cd^{2+} coordination. The time constant for the bridge formation in the open state was 34 s, while no bridge formation occurred in the inactivated state (Fig. S4). This suggests that 325 and 364 are close to each other in the open state and move apart during slow inactivation; consistent with the idea that S4 is relaxing following activation [9].

The metal-ion bridges suggest a long translational movement between S3 and S4. The long stretch of residues in S4 we have identified to make close contact with residues 325 and/or 326 in S3 suggests that S4 slides a considerable distance along S3 during gating (Fig. 3E). In addition to the open state interactions, the rest of the diagram in Fig. 2C shows three distinct regions with a periodicity of three residues, suggesting three non-conducting conformations (C1-C3) that the VSD would pass on the way from fully open to a down state. The diagram suggests that the

325C-361C interaction occurs in the last state before opening (C1). The sliding-helix model predicts that this interaction should be broken at more negative voltages. Indeed, both the making and the breaking of the bridge were clearly voltage dependent, thus supporting the idea of C1 as a distinct pre-open intermediate conformation (Fig. 3F, Fig. S5). The interactions proposed to occur in C2 and C3 were difficult to kinetically separate from each other, suggesting more flexible states further away from the open state, with C3 as the likely candidate for the down state (since C1/C2 would not provide sufficient gating charge). Since some studies [28] have suggested there could be a deeper closed state (C4) reachable in some cases, we additionally investigated whether 352C (one helical turn outside 355) interacts with 325C. Cd²⁺ on 325C/352C reduced the current but the interaction was not as strong as for the other residues and it was independent of state (Fig. S6). Our interpretation is that this part is flexible enough in the Shaker channel to form a bond at any voltage, making it difficult to conclusively isolate a C4 state from contacts between these residues. Instead, we searched for interactions deeper in S3. In a potential C4, 355 should interact with 322, or 358 with either 318 or 319. 322C/355C did not express very well and was thus not possible to investigate. 318C/358C expressed well, but the Cd²⁺ effects were not different from those of the single mutant 358C. In contrast, 319C/358C was readily affected by Cd²⁺; the current at the end of a 100-ms pulse to 0 mV was reduced by $58 \pm 7\%$ ($n = 5$) while neither of the single mutants 319C or 358C were significantly reduced by the same protocol. Thus we conclude that the Shaker K channel goes through at least the C1-C2-C3 sequence of conformations during closing, and in some cases it appears to be possible to capture the VSD in a C4 conformation.

Atomic-resolution models of the different states. For each state, models were built based solely on the experimental information, without any *a priori* assumption of the position of S4. Models were constructed by applying metal-ion bridge constraints in a multi-stage refinement process (see Methods) followed by ten different 100 ns molecular dynamics simulations in a lipid bilayer for each state (Fig. S7) without any constraints applied. An additional set of simulations was performed with Cd²⁺ ions included to assess the influence of the metal-ion bridges on the structure. The distortion of the VSD from the ion was small (Fig. S7), but the strong electrostatic interaction also makes the metal-ion bridges unlikely to break (the S to Cd²⁺ distance is typically 2.23 ± 0.05 Å for all states). For this reason, we consider it a more stringent test whether the intermediate states simulated without ion bridges still fulfill the distance restraints from our experiments. Since the cysteine sulfurs are free to rotate around the C α -C β bond the distances between cysteine C β atoms were observed, which should fall inside ~ 9 Å to be compatible with a bridge when the C β -S γ bond lengths are taken into account. All models fulfill these metal-ion distance constraints during the last 50 ns of unrestrained simulation (Table S2, Fig. S7). To predict specific conformations, the simulations results were clustered in two steps, and the most populated clusters selected (Fig. 4, Table S2). In particular the separation between the C3/C4 states is important. The mere fact the experimental constraints naturally produce different conformations does not by itself mean it is absolutely necessary to have different states. However, neither the present C3 state nor the average conformation of the qualitatively similar recent consensus down state [30] appear to fulfill the constraints as well as C4. The shortest N δ/ϵ -N δ/ϵ distance for residues A359H-I287H (Lin *et al.*, metal-ion bridges [28]) is over 10 Å both in our C3 model and the consensus model, while it is under 4 Å in C4. Similarly, the C β -C β distance for A319C-L358C constraint is 10.2 Å in C3, but 5.9 Å in C4. The consensus model stops just before the residue corresponding to L358, but if modeled it would be

directed away from the side of the helix facing A319, although it is likely the model would not distort a lot if this distance constraint was added. New omega current data from Lehmann *et al.* [31] suggests R362 opposes E293 in the most closed state although Pless *et al.* [32] argue E293 does not engage in state-dependent electrostatic interactions. For these residues the C β distance would be 10.4Å in C4, while it is 14Å in C3 and 15.3Å in the consensus model. For the two latter models the involved residues would even be on opposite sides of F290 (making contact unlikely), while they are naturally adjacent for C4. However, there is presently no evidence it is functionally necessary for VSDs to always adopt this state in a normal VSD cycle, since C3 would produce sufficient gating charge, and VSDs without the final arginine might not even be able to reach C4. PDB structures of the models are available from the authors upon request, and can be downloaded directly at http://www.tcblab.org/henrion_vsd_models/.

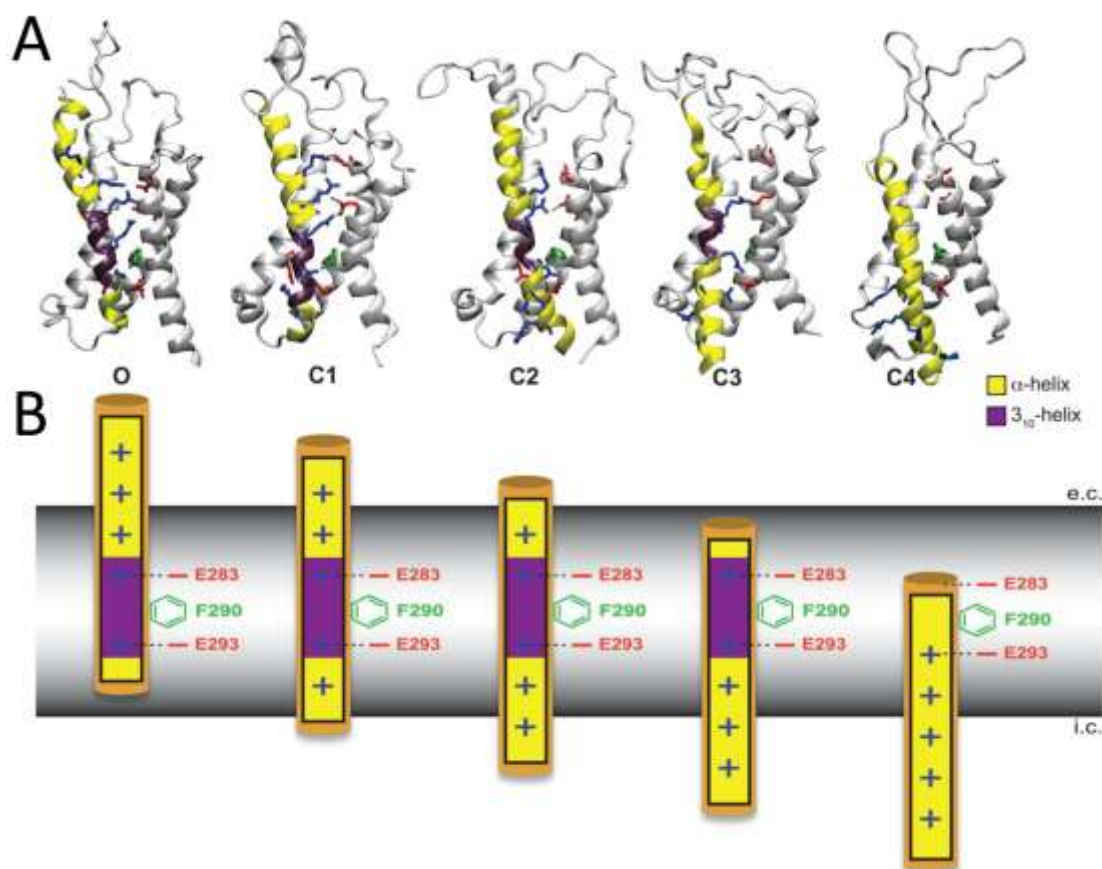


Fig. 4. Molecular models of VSD states and the gating process. (A) Metal-ion constraints and molecular simulation relaxation predicts each C1 through C3, and under some conditions C4, state to correspond to one additional arginine side chain in S4 (blue sticks) translating across the hydrophobic zone lock formed by F290 (green sticks), forming salt bridges to negatively charged residues in S1-S3 (red sticks; E247 in S1 and E283 in S2 above F290, and E293 in S2 and 316D in S3 below F290). The region of S4 close to F290 adopts 3_{10} -helix (purple) in all models but C4, with the rest of S4 in α -helix (yellow). This suggests a gating model where a virtually constant-length 3_{10} -helix region slides along the sequence of S4 without any net free energy cost, which avoids overall rotation of the entire S4 helix during gating – only the outer ends rotate. (B) Cartoon highlighting some of the features from A.

The Shaker O state adopts 3_{10} -helix secondary structure for residues 368-378, similar to the chimera template. The initial model of C1 only contains three residues of 3_{10} -helix around R3 (=R368), but in the model from the molecular dynamics clustering this expands to residues 367-377, i.e. downstream of R3 (=R368). For C2, the 3_{10} -helix region has moved and covers R2-R4 (=R365-R371), and in C3 it moves another three positions to R1-R3 (=R362-R368). For all these conformations, the region of S4 below the 3_{10} -helix converts back into α -helix, with the arginine above F290 forming salt bridges to E283 and the arginine below F290 to E293, both in S2 (Fig. 4). The strain induced by these salt bridges appears to be a main stabilizing factor for the 3_{10} -helix region. These structures suggest a sequence of events for the C1-C2-C3 conformations, which would help explain the rapid transition (although it should be noted that the experimental constraints for C1 & C2 are not very well separated). In contrast, for the C4 model the final R1 side chain has moved below the hydrophobic lock formed by F290, and without any salt bridge to E283 the structure relaxes into all α -helix in the model. This would support a gating model where S4 predominantly moves along its axis with a 3_{10} -helix region that slides along the S4 sequence at least from the open state through C3, with one additional arginine translating across the hydrophobic zone for each subsequent closing step, and C3 would then be the default resting state (supported by the gating charge). The larger structural transition required to move from C3 to C4 could indicate this state might be more difficult, but sometimes possible, to reach. The structure of the upper part of S4 in the C4 state is less certain since there are no strong experimental constraints specifically favoring α -helix, and a helix moving from C3 might be able to retain some 3_{10} -helix structure. As discussed e.g. in Schwaiger *et al.* [33] the lower stability of 3_{10} -helix is reproduced by force fields, but the sliding 3_{10} -helix would not have any net cost between states O through C3.

Single cysteines coordinate Cd^{2+} together with endogenous glutamates or aspartates. Seven of the single-cysteine mutants were affected by 10 μM Cd^{2+} , suggesting that they may coordinate Cd^{2+} together with endogenous residues. Based on the molecular models (Fig. 4) we evaluated possible interactions. For three evenly spaced residues (356C, 359C, and 362C), Cd^{2+} kept the channel in a closed state; the opening kinetics was slowed down (Fig. 5A) and more positive voltages were needed to open the channel (Fig. 5B). All three residues were close to two glutamates in S1 (E247) and S2 (E283) in states C3 and C4 (Fig. 6A), C2 and C3, and C1 and C2 respectively. 365C is close to this glutamate pair in the O state and interestingly Cd^{2+} opens this channel (Fig. 5B). The Cd^{2+} effects on 356C, 359C and 362C were rescued by mutating E283 or E247 to glutamines (Fig. 6B-E, Table S3, Figs. S8 and S9), confirming that these residues are close to E283 and E247 in three consecutive closed states. For two other mutations, 358C and 361C, Cd^{2+} opens the channel (Fig. 5B). Residues 358C and 361C could possibly interact with a cluster of four negatively charged residues at the top of S3 in the O state. The closeness is shown for 358C and the cluster (Fig. 6F). Neutralizing this cluster deleted the Cd^{2+} effect (Fig. 6G-H, Table S3, Fig. S10), supporting that 358 and 361 are close to EEED333-336 in the O state.

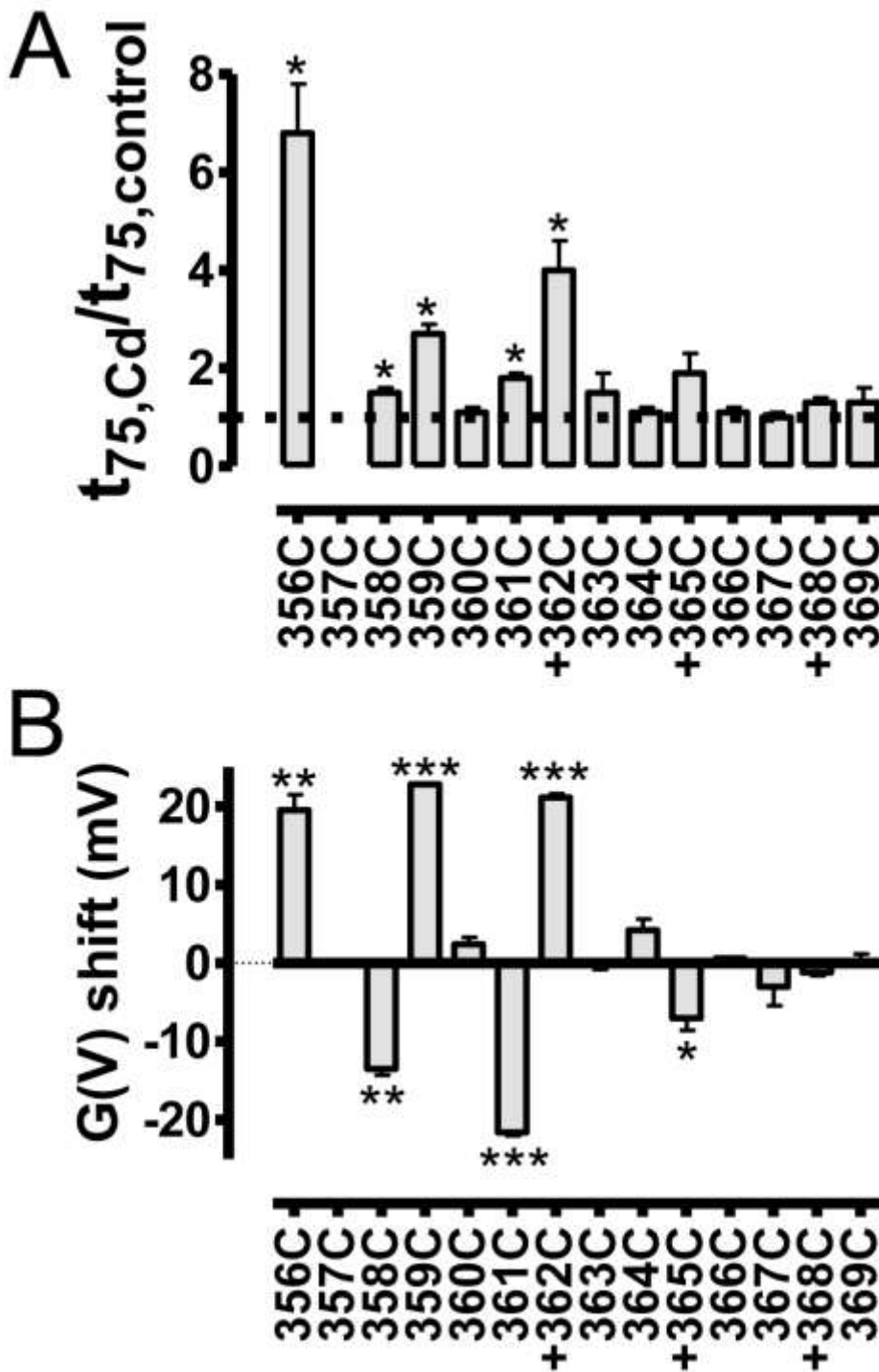


Fig 5. Effects of Cd^{2+} on single cysteine mutants. Summary of Cd^{2+} effects on activation time constants (A) and G(V) shifts (B) of the single mutations. Data shown as mean \pm SEM (n = 2-6). Amplitudes significantly different from 1.0 (A) or 0 (B) are denoted by * if $p < 0.05$, ** if $p < 0.01$, or *** if $p < 0.001$.

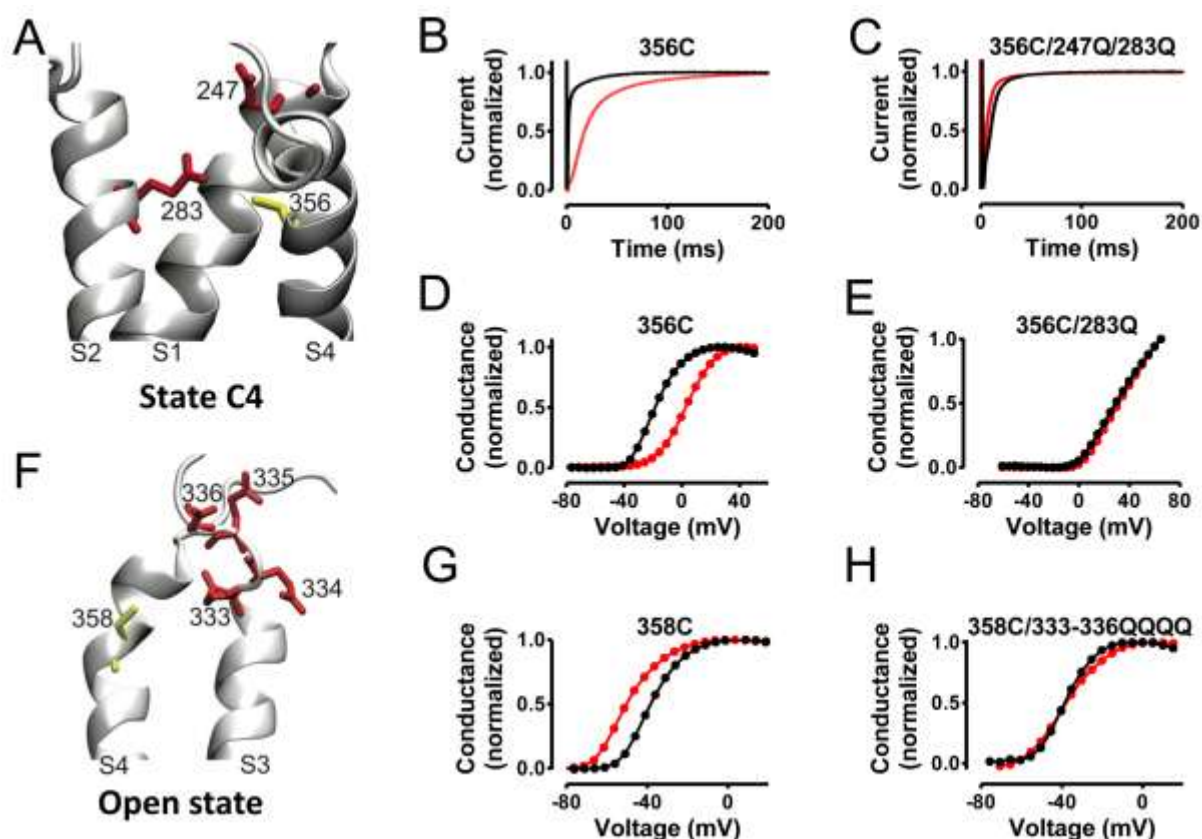


Fig 6. Cd^{2+} is coordinated by one cysteine and two or several negatively charged residues. (A) Glutamates 247 and 283 are close to 356C in the C4-model. (B) Cd^{2+} slows the opening kinetics of 356C. (C) Neutralization of E247 and E283 abolish the Cd^{2+} effect. (D) Cd^{2+} shifts the G(V) of 356C with +19,5 mV (top). (E) Neutralization of E283 abolishes the Cd^{2+} effect. (F) A cluster of negatively charged residues in the S3-S4-linker (E/D333-336) is close to 358C in the O-model. (G) Cd^{2+} shifts the G(V) of 358C with -13.2 mV. (H) Neutralization of E/D333-336 abolishes the Cd^{2+} effect.

DISCUSSION

In the present investigation we have described 20 new interactions between transmembrane segments of the VSD (Table S4). With molecular modeling we have built molecular models of several different intermediate VSD states. These five models are consistent with the interactions described in the present investigation (Table S4) and also fulfill previously published experimental data (Table S5). The open state model, O, with R1-R4 (=R362-R371) outside F290, is close to the previously determined structure of a K channel [5]. Both the C1 and C2 states are compatible with some previous experimental data, and C3 is very similar to previous down-state models [30, 34-36]. The C4 state, with all positive charges inside F290, has S4 even deeper intracellularly, but given the efforts required to capture this state and the fact that C3 is sufficient to explain the gating charge, C4 might only be present at significant hyperpolarization (which could remove it from the normal VSD cycle). Another important finding is that there is a large

relative motion between S3 and S4. The C4 model is consistent with recent experimental data showing that not only R2-R4 (=R365-R361), but also R1 (=R362) might be able to pass inside F290 [28, 31, 37]. The cascading motion of the arginines is similar to recent simulations [38], but in the experimentally derived models this is achieved through a sliding 3_{10} -helix present in all states from O through C3 in the VSD. In the C4 state, the salt bridge to E283 above F290 is lost, and as a consequence S4 relaxes to α -helix in the model. We have also shown that the open state model is transformed to a new configuration during inactivation.

To conclude, our set of models cover a complete sequence of transformations from the deepest closed state to an open state. This set strongly suggests that the VSD activation involves S4 moving at least 12 Å relative to the rest of the VSD (transferring three to four charges across the membrane) from the O to the C3 state, and that it could be possible to reach an even more closed C4 state in some cases with larger structural changes (although this would require a 17 Å motion). The motion can primarily be defined as a sliding helix, and for O through C3 there is a constant-length 3_{10} -helix region moving along the sequence of S4 to maintain its location in the hydrophobic region around F290 of the VSD. The structural difference as well as vertical translation is larger between C3 and C4 compared to the other states. It is an important question whether C3 or C4 is more likely to correspond to the resting state. Considering the Cole-Moore effect where significant hyperpolarization makes it harder to subsequently activate the channel [39], this could be explained by C3 being the default resting state (supported by recent simulations of ω -currents [40]), while C4 might only be reached after long hyperpolarization. This would agree well with the model of a more natural motion from O through C3, while C3 to C4 requires a larger change, and could help reconcile many of the different constraints observed in experiments and models.

METHODS

Oocytes and expression. All experiments were performed on the Shaker H4 channel (Acc No NM_167595.3) [41] made incapable of fast inactivation by the $\Delta(6-46)$ deletion [42]. *Xenopus laevis* surgery, oocyte dissection, channel mutagenesis and cRNA preparation and injection were performed as previously described [15]. Injected oocytes were maintained at 11°C in MBS solution [15] containing pyruvate and antibiotics until subject to electrophysiological experiments. For double-cysteine mutants, 0.5 mM dithiothreitol (DTT) was added to the MBS solution to prevent disulfide-bond formation during incubation.

Electrophysiology. Currents were measured with the two-electrode voltage-clamp technique (CA-1B amplifier, Dagan Corporation, Minneapolis, MN) 3-6 days after injection. The amplifier's leak and capacitance compensation were used and the currents were low-pass filtered at 5 kHz. All experiments were done in room temperature (20-23°C). The control solution contained (in mM): 88 NaCl, 1 KCl, 15 HEPES, 0.4 CaCl₂, and 0.8 MgCl₂. pH was adjusted to 7.4 with NaOH yielding a final sodium concentration of ~100 mM. Solutions of 10 μ M CdCl₂ (if not stated otherwise) were prepared in control solution. To study channel voltage dependence and kinetics, steady-state currents were achieved by stepping to voltages typically between -80 and +50 mV in 5 mV increments from a holding voltage of -80 mV. For mutants with substantially altered voltage dependence, the voltage range was shifted accordingly. Cd²⁺ was applied during 0.1 or 1 s pulses by stepping from a holding voltage of -80 to +20 mV. For other

pulse protocols, please refer to the details in corresponding figure legend. WT channels were essentially inert to 10 μM Cd^{2+} (Table S1). All chemicals are from Sigma-Aldrich, Stockholm, Sweden if not stated otherwise.

Analysis of electrophysiological data. All data analysis was carried out in Clampfit (Version 10.2, MDS Analytical Technologies) or Graphpad Prism (Versions 4.03 and 5.04 for Windows, GraphPad Software, Inc). The conductance, G , was calculated from the steady-state currents, I , according to $G = I / (V - V_{\text{eq}})$, where V is the membrane potential and V_{eq} the reversal potential for K^+ (-80 mV). The Cd^{2+} -induced shifts were determined at 50% of the maximum conductance. The activation speed was assessed by determining the time needed to reach 75% of the maximum current amplitude. For the analysis of 325C/358C in Fig. 3 we decomposed the $G(V)$ curve in two Boltzmann expressions, one following the control $G(V)$ and one assumed to be affected by Cd^{2+} . Similarly, we also decomposed the activation time course in two independent time courses and measured the time constant. However, in Table S1 we used the same analysis as for all other mutations.

Rosetta modeling. A homology model of the voltage sensing domain of Shaker was built by aligning the sequence of Shaker to the sequence of crystal structure of the Kv1.2-Kv2.1 paddle chimera (PDB: 2R9R) with HAlign [43] and building the model with Modeller [44]. The sequence identity is over 40%. This initial model was used as a starting point for modeling based on the experiments. A sequence of distinct constraints believed to be non-overlapping in structure (Table S4) were selected for the models, and represented as harmonic distance restraints centered at 6 Å between the cysteine sulfurs involved in Cd binding. The entire S3-S4 loop as well as the S4 segment (residues 332-379) were rebuilt completely from fragments in Rosetta, allowing the S4 helix to adopt different positions relative to the membrane. The transmembrane backbone of S1-S3 was restrained and only their side chains modified. To enhance sampling of realistic models during the Rosetta step, a weak constraint was also used to keep the arginine residues (R1-R4 (=R362-R371)) in S4 close to the negatively charged E247, E293, or D319. In each modeling stage 10,000 models were sampled, they were subsequently clustered using 2 Å RMSD between the membrane regions, and the model from the largest cluster with the lowest energy was selected.

Molecular dynamics. The simulation systems were generated by superimposing each VSD model onto the structure of an already equilibrated system of a VSD-membrane system [33] simulated in a hexagonal unit cell. Overlapping molecules within 1 Å around the protein were deleted, such that in general 43 lipids per monolayer and about 6900 water molecules remained. The system was neutralized by randomly replacing two water molecules with K^+ counter ions. The final configuration comprises about 28,000 atoms. The VSD was described with the Amber99SB-ILDN force field [45], POPC interactions were described with the Berger force field parameters [46] using united atoms in the tails to reduce the number of particles, and water with the TIP3P model [47]. The systems were energy minimized with steepest descent for 1,000 steps. Subsequently, a short equilibration simulation of 100 ps was performed restraining the water molecules along the z-axis and the protein backbone restrained to its initial position. It was followed by yet another 100 ps of equilibration without restraints on the water molecules. No restraints were applied to maintain the experimental salt bridge distances in the model simulations, but explicit ions were included in a similar set of control simulations.

All simulations were carried out with Gromacs version 4.5.3 [48] package using virtual interaction sites, 4 fs time steps, and all bond lengths constrained. Electrostatic interactions were evaluated using particle mesh Ewald (PME) summation every step. A 10 Å cutoff was used for electrostatics and van der Waals interactions with neighbor lists updated every 10 steps. Simulations were performed at 300 K by using a Bussi thermostat [49]. Semi-isotropic pressure coupling was used, with a Parrinello-Rahman barostat [50] using a time constant of 5 ps and a compressibility of $4.5 \cdot 10^{-5} \text{ bar}^{-1}$ in both the plane of the membrane and along the membrane normal.

Ten 100 ns production runs with different random seeds for velocities were performed for each state, without any restraints on the system. RMSD clustering was performed with the Gromacs `g_cluster` program with a 0.7 Å cutoff, using frames spaced 1 ns apart from the last 50 ns of each simulation, after which centroids from different simulations were clustered with a 2 Å cutoff. The centroid of the most populated cluster was selected as the final model for each state.

ACKNOWLEDGEMENTS

We thank Ingrid Walan and Mattias Larsson for some of the experiments, and Peter Larsson and Gunnar von Heijne for comments on the manuscript. This work was supported by the Swedish Research Council, the Swedish Heart-Lung Foundation, the Swedish Brain Foundation, the County Council of Östergötland, Queen Silvia's Anniversary Foundation, King Gustaf V and Queen Victoria's Freemasons Foundation, Stina and Birger Johansson's Foundation, the Swedish Society for Medical Research, the Swedish Foundation for Strategic Research and the European Research Council.

REFERENCES

1. Borjesson, S.I. and F. Elinder, *Structure, function, and modification of the voltage sensor in voltage-gated ion channels*. Cell Biochem Biophys, 2008. **52**(3): p. 149-74.
2. Schoppa, N.E., et al., *The size of gating charge in wild-type and mutant Shaker potassium channels*. Science, 1992. **255**(5052): p. 1712-5.
3. Zagotta, W.N., T. Hoshi, and R.W. Aldrich, *Shaker potassium channel gating. III: Evaluation of kinetic models for activation*. J Gen Physiol, 1994. **103**(2): p. 321-62.
4. Keynes, R.D. and F. Elinder, *Modelling the activation, opening, inactivation and reopening of the voltage-gated sodium channel*. Proc Biol Sci, 1998. **265**(1393): p. 263-70.
5. Long, S.B., et al., *Atomic structure of a voltage-dependent K⁺ channel in a lipid membrane-like environment*. Nature, 2007. **450**(7168): p. 376-82.
6. Papazian, D.M., et al., *Electrostatic interactions of S4 voltage sensor in Shaker K⁺ channel*. Neuron, 1995. **14**(6): p. 1293-301.
7. DeCaen, P.G., et al., *Disulfide locking a sodium channel voltage sensor reveals ion pair formation during activation*. Proc Natl Acad Sci U S A, 2008. **105**(39): p. 15142-7.
8. DeCaen, P.G., et al., *Sequential formation of ion pairs during activation of a sodium channel voltage sensor*. Proc Natl Acad Sci U S A, 2009. **106**(52): p. 22498-503.
9. Villalba-Galea, C.A., et al., *S4-based voltage sensors have three major conformations*. Proc Natl Acad Sci U S A, 2008. **105**(46): p. 17600-7.
10. Murata, Y., et al., *Phosphoinositide phosphatase activity coupled to an intrinsic voltage sensor*. Nature, 2005. **435**(7046): p. 1239-43.
11. Sasaki, M., M. Takagi, and Y. Okamura, *A voltage sensor-domain protein is a voltage-gated proton channel*. Science, 2006. **312**(5773): p. 589-92.
12. Ramsey, I.S., et al., *A voltage-gated proton-selective channel lacking the pore domain*. Nature, 2006. **440**(7088): p. 1213-6.
13. Ashcroft, F.M., *Ion Channels and Disease*. 1st Ed. ed1999: Academic Press.
14. Sokolov, S., T. Scheuer, and W.A. Catterall, *Gating pore current in an inherited ion channelopathy*. Nature, 2007. **446**(7131): p. 76-8.
15. Borjesson, S.I., et al., *Electrostatic tuning of cellular excitability*. Biophys J, 2010. **98**(3): p. 396-403.
16. Catterall, W.A., et al., *Voltage-gated ion channels and gating modifier toxins*. Toxicon, 2007. **49**(2): p. 124-41.
17. Catterall, W.A., *Ion channel voltage sensors: structure, function, and pathophysiology*. Neuron, 2010. **67**(6): p. 915-28.
18. Borjesson, S.I. and F. Elinder, *An electrostatic potassium channel opener targeting the final voltage sensor transition*. J Gen Physiol, 2011. **137**(6): p. 563-77.
19. Hessa, T., S.H. White, and G. von Heijne, *Membrane insertion of a potassium-channel voltage sensor*. Science, 2005. **307**(5714): p. 1427.
20. Payandeh, J., et al., *The crystal structure of a voltage-gated sodium channel*. Nature, 2011. **475**(7356): p. 353-8.
21. Schoppa, N.E. and F.J. Sigworth, *Activation of Shaker potassium channels. III. An activation gating model for wild-type and V2 mutant channels*. J Gen Physiol, 1998. **111**(2): p. 313-42.
22. Larsson, H.P. and F. Elinder, *A conserved glutamate is important for slow inactivation in K⁺ channels*. Neuron, 2000. **27**(3): p. 573-83.
23. Broomand, A. and F. Elinder, *Large-scale movement within the voltage-sensor paddle of a potassium channel-support for a helical-screw motion*. Neuron, 2008. **59**(5): p. 770-7.
24. Careaga, C.L. and J.J. Falke, *Thermal motions of surface alpha-helices in the D-galactose chemosensory receptor. Detection by disulfide trapping*. J Mol Biol, 1992. **226**(4): p. 1219-35.

25. Webster, S.M., et al., *Intracellular gate opening in Shaker K⁺ channels defined by high-affinity metal bridges*. Nature, 2004. **428**(6985): p. 864-8.
26. Campos, F.V., et al., *Two atomic constraints unambiguously position the S4 segment relative to S1 and S2 segments in the closed state of Shaker K channel*. Proc Natl Acad Sci U S A, 2007. **104**(19): p. 7904-9.
27. Li, M., et al., *Gating the pore of P2X receptor channels*. Nat Neurosci, 2008. **11**(8): p. 883-7.
28. Lin, M.C., et al., *R1 in the Shaker S4 occupies the gating charge transfer center in the resting state*. J Gen Physiol, 2011. **138**(2): p. 155-63.
29. Rulisek, L. and J. Vondrasek, *Coordination geometries of selected transition metal ions (Co²⁺, Ni²⁺, Cu²⁺, Zn²⁺, Cd²⁺, and Hg²⁺) in metalloproteins*. J Inorg Biochem, 1998. **71**(3-4): p. 115-27.
30. Vargas, E., F. Bezanilla, and B. Roux, *In search of a consensus model of the resting state of a voltage-sensing domain*. Neuron, 2011. **72**(5): p. 713-20.
31. Lehmann, C., H. Heldstab, and N.G. Greeff, *Positioning and Guidance of the Voltage Sensor S4 Within the Omega/Gating-Pore in the Shaker K-Channel*. Biophys J., 2012. **102**(3): p. 532a.
32. Pless, S.A., et al., *Contributions of counter-charge in a potassium channel voltage-sensor domain*. Nat Chem Biol, 2011. **7**(9): p. 617-23.
33. Schwaiger, C.S., et al., *3-helix conformation facilitates the transition of a voltage sensor S4 segment toward the down state*. Biophys J, 2011. **100**(6): p. 1446-54.
34. Khalili-Araghi, F., et al., *Calculation of the gating charge for the Kv1.2 voltage-activated potassium channel*. Biophys J, 2010. **98**(10): p. 2189-98.
35. Schow, E.V., et al., *Down-state model of the voltage-sensing domain of a potassium channel*. Biophys J, 2010. **98**(12): p. 2857-66.
36. Pathak, M.M., et al., *Closing in on the resting state of the Shaker K(+) channel*. Neuron, 2007. **56**(1): p. 124-40.
37. Tao, X., et al., *A gating charge transfer center in voltage sensors*. Science, 2010. **328**(5974): p. 67-73.
38. Delemotte, L., et al., *Intermediate states of the Kv1.2 voltage sensor from atomistic molecular dynamics simulations*. Proc Natl Acad Sci U S A, 2011. **108**(15): p. 6109-14.
39. Cole, K.S. and J.W. Moore, *Potassium ion current in the squid giant axon: dynamic characteristic*. Biophys J, 1960. **1**: p. 1-14.
40. Khalili-Araghi, F., et al., *Molecular Dynamics Investigation of the omega-Current in the Kv1.2 Voltage Sensor Domains*. Biophys J, 2012. **102**(2): p. 258-67.
41. Kamb, A., J. Tseng-Crank, and M.A. Tanouye, *Multiple products of the Drosophila Shaker gene may contribute to potassium channel diversity*. Neuron, 1988. **1**(5): p. 421-30.
42. Hoshi, T., W.N. Zagotta, and R.W. Aldrich, *Biophysical and molecular mechanisms of Shaker potassium channel inactivation*. Science, 1990. **250**(4980): p. 533-8.
43. Soding, J., *Protein homology detection by HMM-HMM comparison*. Bioinformatics, 2005. **21**(7): p. 951-60.
44. Sali, A. and T.L. Blundell, *Comparative protein modelling by satisfaction of spatial restraints*. J Mol Biol, 1993. **234**(3): p. 779-815.
45. Lindorff-Larsen, K., et al., *Improved side-chain torsion potentials for the Amber ff99SB protein force field*. Proteins, 2010. **78**(8): p. 1950-8.
46. Berger, O., O. Edholm, and F. Jahnig, *Molecular dynamics simulations of a fluid bilayer of dipalmitoylphosphatidylcholine at full hydration, constant pressure, and constant temperature*. Biophys J, 1997. **72**(5): p. 2002-13.
47. Jorgensen, W.L., et al., *Comparison of simple potential functions for simulating liquid water*. J. Chem. Phys., 1983. **79**: p. 926-935.

Henrion et al.

48. Hess, B., et al., *GROMACS 4.0: Algorithms for highly efficient, load balanced, and scalable molecular simulation*. J. Chem. Theory Comp., 2008. **4**(2): p. 435.
49. Bussi, G., D. Donadio, and M. Parrinello, *Canonical sampling through velocity rescaling*. J. Chem. Phys., 2007. **126**: p. 014101.
50. Parrinello, M., *Polymorphic transitions in single crystals: A new molecular dynamics method*. J. Appl. Phys, 1981. **52**: p. 7182.